Food and Chemical Toxicology 127 (2019) 197–205

Contents lists available at ScienceDirect

Food and Chemical Toxicology

journal homepage: www.elsevier.com/locate/foodchemtox

Combination of bioanalytical approaches and quantitative proteomics for the elucidation of the toxicity mechanisms associated to TiO_2 nanoparticles exposure in human keratinocytes

Sandra Montalvo-Quiros[a,b], Jose L. Luque-Garcia[a,*]

[a] Department of Analytical Chemistry, Faculty of Chemical Sciences. Complutense University of Madrid, 28040, Madrid, Spain
[b] Centre of Technological and Social Studies (CETYS), Francisco de Vitoria University, 28223, Pozuelo de Alarcón, Madrid, Spain

ARTICLE INFO

Keywords:
TiO_2 nanoparticles
Toxicity mechanisms
Quantitative proteomics

ABSTRACT

Titanium dioxide nanoparticles (TiO_2-NPs) are being used in several consumer products. The high refractive index of nano-scaled titanium dioxide particles allows them to protect from UV radiation, and so, they can be found as one of the main components of cosmetics and suncreens. Many studies have reported the potential toxicological effects associated to TiO_2-NPs such as ROS generation, DNA damage, apoptosis and cell cycle arrest, among others. The continuous and systematic use of TiO_2-NPs in cosmetic products requires a full comprehension of the risks involving their sustained contact with the human skin. Thus, it is important to evaluate not only the hazardous effects but to elucidate the biomolecular mechanisms involved in such effects. Based on this premises, we have evaluated the potential toxicity of TiO_2-NPs using a human epithelial cell culture (HaCaT cells) as in-vitro model, together with different bioanalytical approaches and mass spectrometry-based quantitative proteomics, to gain a deeper insight into the molecular mechanisms of toxicity associated to TiO_2-NPs exposure.

1. Introduction

Titanium dioxide nanoparticles (TiO_2-NPs) belong to a large group of metallic nanoparticles. These nanoparticles have been increasingly used in a variety of consumer products, such as cosmetics and sunscreens, paints and surface coatings. Compared to macrosized particles (MPs > 100 nm), nanoparticles (< 100 nm) show specific properties, including large surface area per unit mass, small size and high reactivity. For these reasons, there is a potentially harmful risks to human health when nanoparticles are inhaled, ingested or in contact with the skin (Iavicoli et al., 2011; Shi et al., 2013). TiO_2 is found in three crystalline phases (rutile, anatase and brookit) but only the first two crystal structures are used in industry. Several studies have shown different toxicity responses depending on the crystal form in different cell lines (Saquib et al., 2012; Gerloff et al., 2012; Wang et al., 2015; Uboldi et al., 2016; Jain et al., 2017), and in most cases, anatase phase exhibited the highest toxicity compared to the others. Among the most commonly described cytotoxic effects induced by TiO_2-NPs are: ROS generation, DNA damage (Saquib et al., 2012; Wang et al., 2015), apoptosis, cell cycle arrest (Wu et al., 2010; Kansara et al., 2015) and increased inflammatory response (Han et al., 2013).

In particular, the use of TiO_2-NPs in sunscreens and cosmetics makes relevant the study of their potential toxicity and hazardous effects in human skin, since they are in close contact for long periods of time. Previous reports, have evaluated the cytotoxicity (Wright et al., 2017), genotoxicity (Jaeger et al., 2012) or metabolic effects (Tucci et al., 2013; Ren et al., 2018) of TiO_2-NPs in human keratinocytes. However, a further evaluation to gain a deeper insight into the biomolecular mechanisms related to those observed effects have not yet been accomplished.

Among the different existing alternatives in quantitative proteomics, stable isotopic labeling by amino acids in cell culture (SILAC), remains one of the most widely used approaches. In SILAC, cell populations are differentially labeled with either $^{12}C_6$-Lys/Arg (light culture) or $^{13}C_6$-Lys/Arg (heavy culture). After complete labeling, the two cell cultures subjected to different conditions (e.g. control vs. Exposure) are mixed in a 1:1 ratio and processed (protein purification, separation, digestion, etc.) as one sample. This procedure allows for the quantification of differentially expressed proteins with high accuracy, thus allowing for the identification of altered or deregulated proteins (overexpressed or inhibited) between the two studied cellular conditions (Luque-Garcia et al., 2013).

* Corresponding author.
E-mail address: jlluque@ucm.es (J.L. Luque-Garcia).

https://doi.org/10.1016/j.fct.2019.03.036
Received 26 December 2018; Received in revised form 27 February 2019; Accepted 19 March 2019
Available online 22 March 2019
0278-6915/

Based on all of the above, in the present work, we first investigated the toxicity of TiO_2-NPs in human keratinocytes (HaCaT cell line) using bioanalytical approaches to evaluate cell viability, cellular uptake, apoptosis, and changes in the cell cycle pattern and in key regulators involved in cell cycle progression. This study was followed by a quantitative proteomic experiment using SILAC, with the aim to move forward and to identify specific proteins and pathways altered upon TiO_2-NPs exposure, which are the ultimate responsible of the toxicity effects observed in exposed human keratinocytes.

2. Materials and methods

2.1. Materials

Commercial anatase titanium dioxide nanoparticles (TiO_2-NPs) with < 25 nm particles size, MTT reagent, dimethyl sulfoxide (DMSO), Hoechst 33258 reagent and tubulin primary antibody were purchased from Sigma Aldrich. Dulbecco's modified Eagle's medium (DMEM), fetal bovine serum (FBS), penicillin/streptomycin, 0.1% trypsin/EDTA solution and phosphatase saline buffer (PBS) were obtained from Thermo Fisher Scientific. Cell culture mediums, LM011 and LM014, for SILAC experiment were purchased from DC Biosciences. FITC-Annexin V/PI kit and p21 primary antibody were obtained from Invitrogen and Santa Cruz, respectively.

For the characterization of these NPs, two stock solutions of 200 and 1000 mg/L, were prepared in Milli-Q water and analyzed by transmission electron microscopy (JEOL 2100). All reagents used to evaluate the localization of NPs in cells were supplied by the microscopy analysis center (CNME). All samples analyzed by flow cytometry were measured using a FACScan flow cytometer (Becton-Dickinson).

For gene expression assays, TRIzol reagent, Quantitect reverse transcription kit, TaqMan gene expression assays and TaqMan Fast advance master mix were purchased from Invitrogen, Quiagen and Thermo Fisher Scientific, respectively. Nanodrop One (Thermo Fisher Scientific) was used to quantify RNA and PikoReal Real-time PCR system (Thermo Scientific) was used to performed RT-PCR analysis. Liquid chromatography tandem-mass spectrometry (LC-MS/MS) was carried out using an LTQ XL ion trap mass spectrometer (Thermo Scientific) coupled to a 1D-nanoLC (Eksigent).

2.2. Cell culture and treatment

The human keratinocyte cell line (HaCaT, Human adult low Calcium High Temperature Keratinocytes) was maintained in Dulbecco's modified Eagle's medium (DMEM) supplemented with 10% fetal bovine serum (FBS) and 1% penicillin/streptomycin at 37 °C and 5% CO_2. HaCaT cells were exposed to different concentrations of TiO_2-NPs ranging from 1 to 100 mg/L and incubated for 72 h. Cells were rinsed in phosphatase saline buffer (PBS) containing 0.02% EDTA and harvested using 0.1% trypsin/EDTA solution. For the metabolic labeling, cells were cultured in either “light” ($^{12}C_6$-Arg and $^{12}C_6$-Lys) or “heavy” ($^{13}C_6$-Arg and $^{13}C_6$-Lys) DMEM medium supplemented with 10% dialyzed FBS and 100 units/mL of penicillin/streptomycin. Cells were grown for at least eight doubling to allow full incorporation of labeled amino acids.

2.3. Cell viability assay

HaCaT cells were seeded on 96-well plates and exposed to 1, 10, 30 or 100 mg/L of TiO_2-NPs for 72 h. 20 µL of 3-(4,5-dimethyl-thiazol-2-yl) 2,5-diphenyl tetrazolium bromide (MTT, 5 mg/mL) were added to each well and incubated for 4 h. After this time, the MTT solution was removed and 100 µL of dimethyl sulfoxide (DMSO) were added to dissolve the insoluble purple formazan product. The plate was then centrifuge and the supernatant of each well was transferred to a new 96-well plate for the measurement of the absorbance at 595 nm in a microplate reader (TECAN).

2.4. Localization of TiO2-NPs in HaCaT cells

Cells were exposed to TiO_2-NPs (10 mg/L) and incubated at 37 °C in 5% CO_2 for 72 h. Afterwards, the control and TiO_2-NPs exposed cells were harvested, rinsed with PBS and fixed with 5% glutaraldehyde and 4% p-formaldehyde in PBS for 4 h at 4 °C. After this time, cells were washed twice with PBS and incubated in PBS at 4 °C overnight. After incubation with 1% OsO_4 in Milli-Q water for 1 h at room temperature, the samples were washed, dehydrated in a graded series of acetone and embedded in resine for 72 h at 67 °C. Ultrafine sections were cut with an ultramicrotome, deposited onto copper grids, stained with uranyl acetate and chrome citrate and analyzed by transmission electron microscopy (JEOL 1010).

2.5. Flow cytometry assays

Measurement of apoptosis in TiO_2-NPs (10 mg/L) exposed cells after 72 h was determined using an FITC-Annexin V/PI kit (Invitrogen). Cells were harvested and washed with cold PBS. $1x10^6$ cells were resuspended in 1 mL binding buffer solution at pH 7.4 containing 50 mM HEPES, 700 mM NaCl and 12.5 mM $CaCl_2$. 100 µL of the cell suspension was stained with 5 µL of FITC-annexin V and 1 µL of 100 µg/mL propidium iodide. Cells were incubated for 15 min in the dark at room temperature, diluted in 400 µL of binding buffer and immediately examined using a FACScan flow cytometer (Becton-Dickinson). To evaluate the cell cycle pattern of TiO_2-NPs exposed cells, $1x10^6$ cells were suspended in 250 µL of PBS and mixed with the same volume of a solution containing 60% ethanol and 30 µg/mL Hoechst 33258 reagent. Cells were then incubated for 1 h at room temperature in the dark and the DNA content analyzed by flow cytometry.

2.6. Gene expression: RT-qPCR analysis

The mRNA levels of cell cycle related genes (Table 1) were measured in TiO_2-NPs exposed HaCaT cells (10 mg/L and 72 h). Total RNA was isolated using TRIzol reagent (Invitrogen) according to the manufacturer's instructions. The quantity of extracted RNA was measured by the Nanodrop One (Thermo Fisher Scientific). Synthesis of cDNA with integrated removal of genomic DNA contamination was performed by Quantitect reverse transcription kit (Quiagen) using 1 µg of RNA. RT-PCR analysis was carried out using TaqMan gene expression assays (Thermo Fisher Scientific) and TaqMan Fast advance master mix (Thermo Fisher Scientific) according to the manufacturer's instructions. The references of TaqMan gene expression assays used are listed in Table 1. All reactions were performed in a final volume of 10 µL. The reaction protocol was 2 min at 50 °C, 10 min at 95 °C for activating the polymerase and 40 cycles for 15 s at 95 °C and 1 min at 60 °C. Relative expression of genes was normalized using GADPH as the endogenous control and gene expression in each sample was calculated as $2^{-\Delta\Delta Ct}$.

Table 1
Cell cycle related genes studied by RT-qPCR.

Gene	RefSeq	Assay ID
CDK1	NM_001170406.1	Hs00938777_m1
CCNB1	NM_031966.3	Hs01030099_m1
CDK2	NM_001290230.1	Hs01548894_m1
CCNE1	NM_001238.3	Hs01026536_m1
CCNA2	NM_001237.3	Hs00996788_m1
CDKN1A	NM_000389.4	Hs00355782_m1
TP53	NM_000546.5	Hs01034249_m1
GADPH	NM_001256799.2	Hs03929097_g1

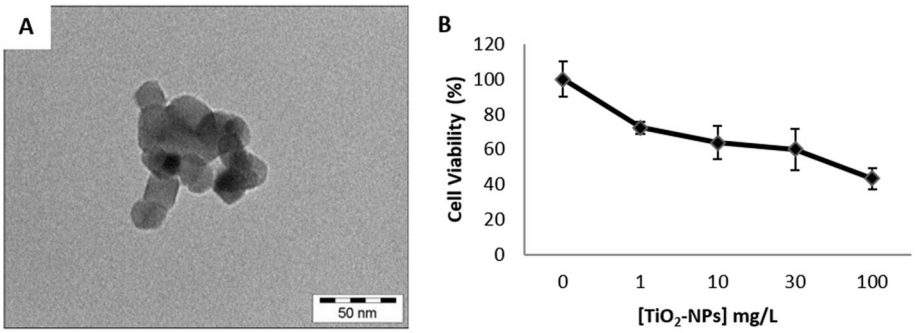

Fig. 1. Morphologic characterization of TiO_2-NPs by TEM and effects of these nanoparticles on HaCaT cell viability after 72h of exposure. (A) NPs show spherical shape and tendency to aggregate. **(B)** The reduction of cell viability after TiO_2-NPs exposure was evaluated at different concentrations (1, 10, 30, 100 μg/mL) by the MTT assay.

2.7. Western blotting

HaCaT cells were lysed with total lysis buffer containing a protease inhibitors cocktail. Protein concentration was determined using the Bradford assay. Proteins were separated by electrophoresis on a 12.5% SDS-polyacrylamide gel and transferred to a nitrocellulose membrane (BioRad). Membrane was blocked with 3% skim milk in PBS-T (0.05% Tween-20) for 1 h at room temperature. After blocking, membrane was incubated with the primary antibodies diluted in blocking buffer: tubulin 1:500 (Sigma Aldrich) for 1 h at room temperature and p21 1:200 (Santa Cruz) overnight at 4 °C. After three 10 min washes, the membrane was incubated with the corresponding secondary antibodies HRP-conjugated for 1 h. The inmunoblot was then visualized by enhanced chemiluminescence detection (GE Healthcare).

2.8. SILAC experiment

Two large-scale SILAC replicates (10^7 cells per condition) were performed. Complete incorporation of $^{13}C_6$-Lys and $^{13}C_6$-Arg after eight cell divisions in isotopically heavy medium was verified by MS of a protein digest (data not shown). HaCaT cells labeled with "heavy" (direct SILAC) or "light" (reversed SILAC) amino acids were exposed to 10 mg/L of TiO_2-NPs for 72 h. Then, cells grown in "heavy" and "light" medium were harvested, counted and mixed in a 1:1 ratio before subsequent processing. Cells were lysed in buffer containing protease inhibitors (Roche) and the protein concentration was determined using the Bradford method. Proteins were then separated by SDS-PAGE on 10% SDS-polyacrylamide gels. After electrophoresis, the proteins were visualized by Coomassie blue staining and the gel lane was cut horizontally into 22 sections. Excised gel bands were de-stained in 25 mM ammonium bicarbonate/50% acetonitrile, cut into small pieces, dehydrated with acetonitrile and dried. Gel pieces were incubated with 12.5 ng/μL trypsin solution in 25 mM ammonium bicarbonate overnight at 37 °C. Peptides were extracted using acetonitrile and 5% formic acid, dried by vacuum centrifugation and reconstituted in 12 μL of an aqueous solution containing 2% acetonitrile and 0.1% formic acid.

The peptides mixtures from different fractions were analyzed using a nanoflow LC-MS/MS. Peptides were loaded onto a C18 trap column (0.3 × 10 mm, SGE) and then separated on a reverse-phase column (75 μm × 25 cm fused silica capillary C18 HPLC PepMap column, 3 μm, 100 A, Thermo) with a linear gradient of 5–95% acetonitrile in 0.1% aqueous solution of formic acid. The gradient was delivered over 120 min by a nano LC ultra 1D plus system (Eksigent) at a flow-rate of 200 nL/min, through the analytical column to a stainless nano-bore emitter (Proxeon). The peptides were scanned and fragmented with an LTQ XL linear ion trap mass spectrometer (Thermo Scientific) operated in data-depend ZoomScan and MS/MS switching mode using the three most intensive precursor ions detected in a survey scan from 400 to 1600 u (three μscans). ZoomScan mass window was set to 12 Da enabling monitoring of the entire $^{12}C/^{13}C$ isotopic envelope of most doubly and triply charged peptides. Singly charged ions were excluded for MS/MS analysis.

Generated .raw files were converted to .mgf files for MASCOT data search. A database containing the NCBInr *Homo Sapiens* sequences (113620 entries as of 03/31/2018) was searched using the MASCOT protein identification software (v2.3 MatrixScience). Search criteria included trypsin specificity with one missed cleavage allowed, and with methionine oxidation, $^{13}C_6$-Arg and $^{13}C_6$-Lys as variable modifications. Minimum precursor and fragment-ion mass accuracies for 1.2 and 0.3 Da were used. To consider a protein as an accurate identification, at least one bold (unique) red peptide (i.e. highest scoring peptide matching to protein with highest total score) was required, and at least two bold (unique) red peptides were required for quantification. Cut-off values for MASCOT scores of peptides and proteins were set to 40 ($p < 0.05$) and 47 ($p < 0.01$), respectively. The false positive rate was calculated by searching the same spectra against the NCBInr *Homo Sapiens* decoy database. Relative quantification ratios (R_{SILAC}) of identified proteins based on peak area were calculated using Quixot (version 1.3.26) open-source software. Protein ratios obtained by QuiXot were manually verified for all peptides. The biological processes related to the proteins found deregulated upon TiO_2-NPs exposure, were assigned based on the biological knowledge available in Gene Ontology (GO) annotations.

3. Results

3.1. Characterization and cytotoxicity of TiO2-NPs

Transmission electron microscopy was used to characterize the TiO_2-NPs in terms of particle size, morphology and aggregation. TiO_2-NPs presented spherical structure with a diameter around 20–30 nm and tendency to aggregate in suspension (Fig. 1A).

The effect of TiO_2-NPs on the cell viability of HaCaT cells was evaluated by means of the MTT assay, which measures the reducing potential of the cells. While healthy cells are able to reduce the MTT to formazan (a purple coloured compound), non-viable cells are unable to do so. Thus, cell viability can be estimated by measuring the absorbance of the MTT-treated cells. As expected, the viability of HaCaT cells exposed to TiO_2-NPs for 72 h, decreased with increasing concentrations of the NPs (Fig. 1B). In order to evaluate the potential toxicity of TiO_2-NPs but without drastically compromising the cell viability, a concentration of 10 mg/L was selected for further experiments.

3.2. Cellular uptake and localization of TiO2-NPs

Transmission electron microscopy (TEM) was used for investigating the internalization and localization of TiO_2-NPs in exposed HaCaT cells (Fig. 2). Several TiO_2-NPs aggregates were found in most of the exposed cells (Fig. 2B). These aggregates, where either found close to the cellular surface, where invaginations of the plasma membrane (Fig. 2C) were observed, or in vacuoles throughout the cytoplasm (Fig. 2B and D). As expected, these TiO_2-NPs were not able to penetrate the nuclear membrane (Fig. 2E). Statistical analysis of 40 cell images (20 control cells and 20 cells exposed to TiO_2-NPs) showed a significant increased

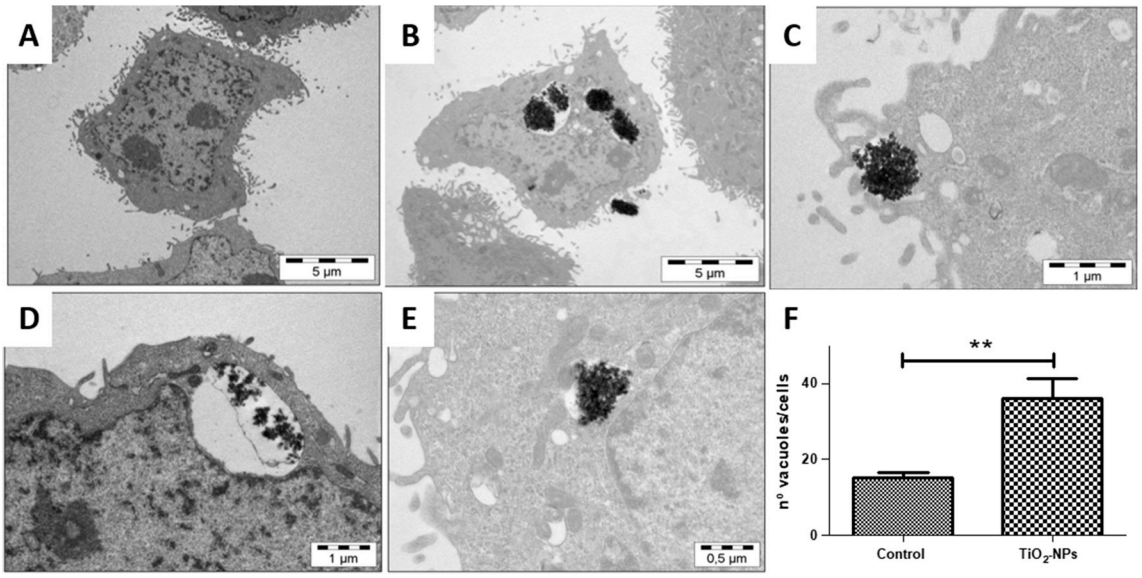

Fig. 2. Transmission electron microscopy of HaCaT cells after TiO_2 -NPs exposure. (B) NPs were found inside exposed HaCaT cells as aggregates when compared to **(A)** control cells. **(C)** Invaginations of the cell membrane were found in cells exposed to TiO_2 –NPs, **(D)** which were located in vacuoles inside the cells. **(E)** These NPs were not able to penetrate the nuclear membrane. **(F)** Treated cells showed higher number of vacuoles as compared to control cells. **p < 0.01.

(more than 2-fold) in the number of vacuoles in exposed cells as compared to control ones (Fig. 2F).

3.3. Flow cytometry assays

Two flow cytometry assays were carried out in order to explain whether the observed decreased in cell viability after exposure to TiO_2-NPs, could be attributed to an increase in cell death or to a cell cycle arrest. The data obtained in both assays are shown in Fig. 3. The results demonstrated that cells exposed to TiO_2-NPs did not show a significant higher degree of apoptosis or necrosis as compared to control cells (Fig. 3A). On the contrary, while evaluating the effects of TiO_2-NPs on the cell cycle pattern, cells exposed to TiO_2-NPs showed a higher percentage of S/G2-M cells as compared to control cells. Also, the cellular population in G0/G1 phase after TiO_2-NPs exposure, was significantly lower than in control cells (Fig. 3B). Thus, it can be concluded that TiO_2-NPs did not induce a significant degree of apoptosis in HaCaT cells but they did induce a significant cell cycle arrest at the S-G2/M phase.

3.4. Gene expression assays

Based on the flow cytometry results and in order to corroborate the cell cycle arrest induced by TiO_2-NPs in HaCaT cells, mRNA levels of several key genes involved in cell cycle regulation were evaluated. Since an increase of cell population was found in the transition from S phase to G2-M phases, the checkpoints and mechanisms involved in these phases (Fig. 4A) were considered. The mRNA levels measured by RT-qPCR in HaCaT cells exposed to TiO_2-NPs are shown in Fig. 4B. As for the components of the G1/S checkpoint, a reduction of CDK2 mRNA level was observed while the expression of cyclin E1 (CCNE1) remained constant. On the other hand, another complex formed by CDK2 and cyclin A1 (CCNA1), which constitute the S/G2 checkpoint was also evaluated. In this case, a decrease in the levels of both transcripts (CDK2 and CCNA1) in TiO_2-NPS exposed cells was observed as compared with control cells (Fig. 4B). In addition, also a transcript involved in the G2/M checkpoint (CCNB1) was found significantly inhibited in cells exposed to TiO_2-NPs.

Cell cycle arrest in response to DNA damage involves protein stabilization and consequent upregulation of p53 (Macleod et al., 1995), which induces transcription of cyclin-dependent kinase inhibitor p21

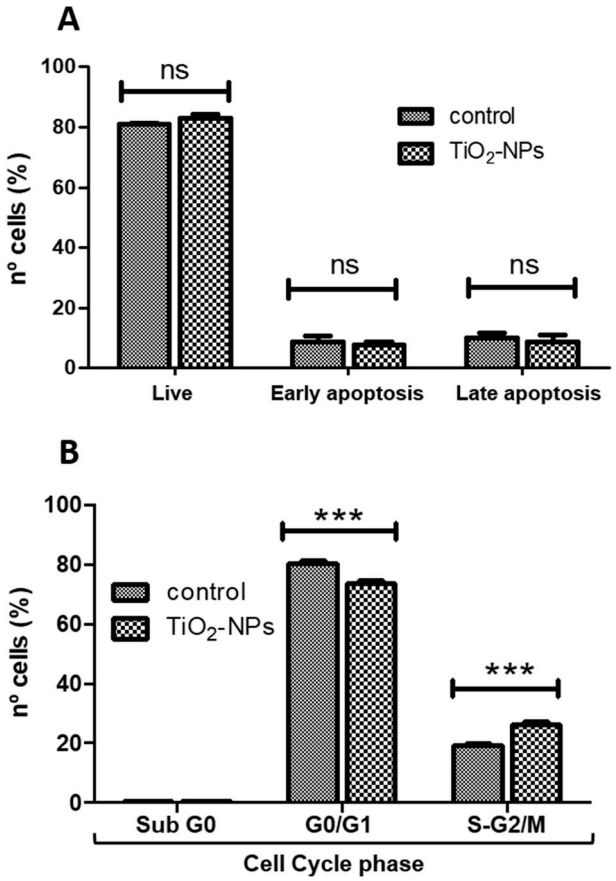

Fig. 3. Flow cytometry assays to evaluate apoptosis and cell cycle pattern in HaCaT cells exposed to TiO_2 -NPs. (A) Annexin-V-based flow cytometry analysis did not reveal a significant increase in apoptosis after the exposure. **(B)** Measurement of the DNA content by flow cytometry shows that the number of cells in S/G2-M significantly increase in TiO_2-NPs exposed cells as compared to control ones. ***$p < 0.001$.

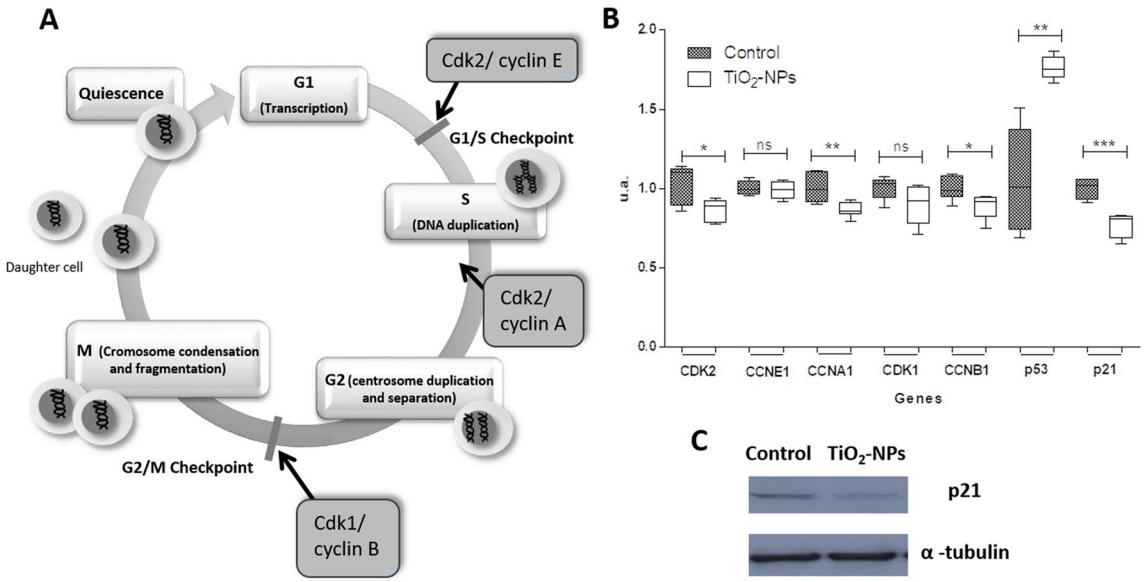

Fig. 4. Gene expression and western blot analysis to evaluate the effects of TiO_2 -NPs exposure in the cell cycle pattern. (A) General scheme showing the essential role of Cdks and cyclins in cell cycle progression. **(B)** mRNA levels of several related-cell cycle genes in control cells and TiO_2-NPs exposed cells. **(C)** Western blow analysis against p21; α-tubulin was used as loading control. $*p < 0.05$, $**p < 0.01$ and $***p < 0.001$.

(Gartel and Tyner, 2002). Thus, mRNA levels of p53 and p21 were also evalauted. As expected, the results showed a significant increase in the expression of p53 in HaCaT cells exposed to TiO_2-NPs. However, a significant decrease in the expression of p21 in exposed cells was observed. This result was not expected since p21 plays an essential role in growth arrest after DNA damage (Dulic et al., 1994). Although this result may appear contradictory, p21 has also been demonstrated to function as a negative regulator of p53 under certain conditions (Broude et al., 2007).

3.5. Western blot assay

To further validate the previous result obtained for p21 mRNA levels and to evaluate its expression at the protein level, an immunoblot was carried out. Cells exposed to TiO_2-NPs also showed a partial inhibition of p21 at the protein level as compared to control cell (Fig. 4C), which is in agreement with the result obtained by RT-qPCR.

3.6. Quantitative proteomics

A SILAC experiment to evaluate the differential protein expression after TiO_2-NPs exposure (Fig. 5A) was performed. A total of 1874 proteins were identified by mass spectrometry analysis with at least one unique peptide and a false discovery rate of 0.35% estimated from the number of hits against reverse or randomised sequence (decoy database)/total hits ratio at $p > 0.01$. However, only 538 proteins passed the selected criteria for quantitation (at least two unique peptides). We then studied the proteins with at least 1.5-fold expression difference between control and exposed cells (R_{SILAC} over +1.5 or below −1.5) and with 20% as the maximum relative standard deviation for the R_{SILAC} between peptides within each protein. According to these criteria, 66 proteins appeared deregulated in cells exposed to TiO_2-NPs as compared to control ones. Out of these proteins, 30 were found upregulated ($R_{SILAC} > 1.5$) (Table 2) and 36 were downregulated ($R_{SILAC} < 1.5$) (Table 3). Regarding the SILAC ratio distribution, most of the identify proteins were within a R_{SILAC} close to 1, as expected for a 1:1 mixture (Fig. 5B). The 67 proteins found deregulated in HaCaT cells exposed to TiO_2-NPs are involved in a variety of biological processes: cell cycle regulation, gene expression, metabolic processes and response to stimulus, among others (Fig. 5C).

4. Discussion

Several previous in vivo and in vitro studies carried out by different research groups have demonstrated that TiO_2-NPs can be absorbed by inhalation, ingestion and penetration through the skin (De Matteis V 2017). Histopathological injuries have been observed mainly in lung, kidney, liver, spleen and the nervous system, among other components of the organism (Iavicoli et al., 2011, Márquez-Ramírez et al 2012, Iavicoli et al., 2012, Chen Z. et al., 2015, Valentini X et al., 2017 and 2018). The toxicological effects they generate have been related to inflammatory responses that result in an increase in reactive oxygen species (ROS) (Saquib et al., 2012; Jaeger et al., 2012; Liu et al., 2010; Khana et al., 2015).

On the other hand, base modification, single or double DNA strand rupture and direct TiO_2 bonds to repair enzymes or DNA can be observed in different models treated with high concentrations of these NPs (Saquib et al., 2012). Additional studies have identified numerous metabolites affected by the cytotoxicity of these NPs which are involved in mitochondrial processes, redox homeostasis as well as in inflammatory responses (Tucci et al., 2013).

The present study has demonstrated the toxicity exerted by TiO_2-NPs on human keratinocytes as well as the main biomolecular mechanisms involved in such toxicity. It has been demonstrated that TiO_2-NPs reduce the cell viability of HaCaT cells in a concentration-dependent manner, in such way that exposure to 10 mg/mL for 72 h decreases the viability by a 40%, approximately. The reduction in viability is accompanied by the cellular uptake of TiO_2-NPs, which form aggregates that localized mainly inside cytoplasmic vacuoles, as it has been shown by TEM. Thus, the degree of vacuolization in keratinocytes exposed to TiO_2-NPs was significantly higher as compared to control cells. Investigations on whether the observed decrease in cellular viability was due to an induction of apoptosis or by a cell cycle arrest was carried out by flow cytometry. The results pointed out that, while TiO_2-NPs did not significantly induce apoptosis, they induced cell cycle arrest at the S-G2/M phase. These results were validated by RT-qPCR. Inhibition of CDK2, CCNA1, CCNB1 was observed, being these genes key regulators of the G1/S, S/G2 and G2/M checkpoints, whose inhibition induce cell cycle arrest, which is in agreement with the results obtained by flow cytometry.

Since cell cycle arrest often involves protein stabilization and

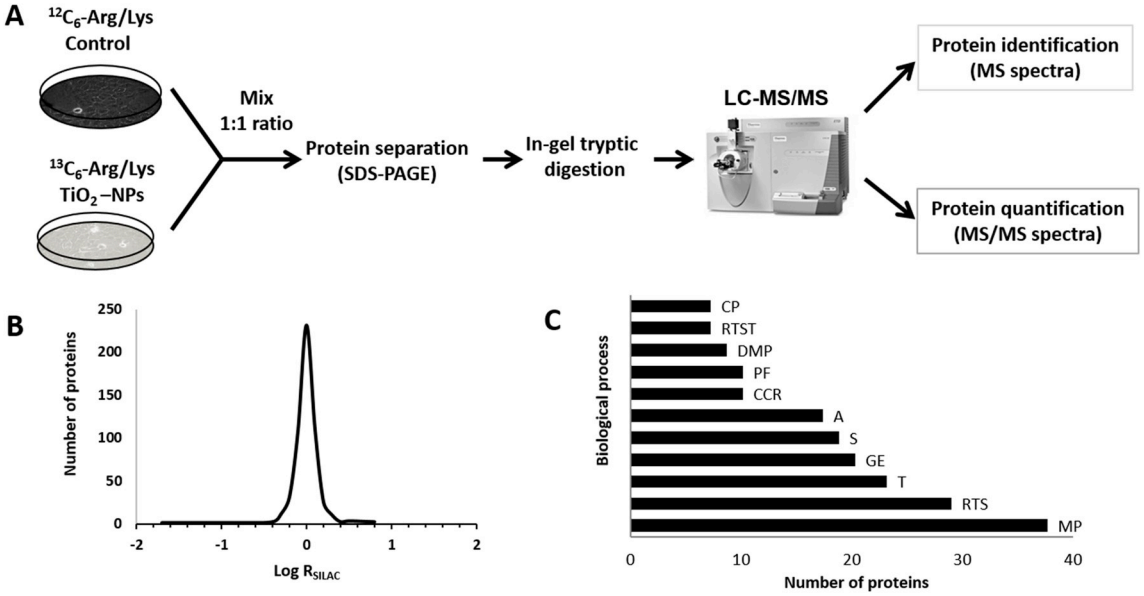

Fig. 5. SILAC results. (A) General scheme of the SILAC experiment procedure. **(B)** Distribution of the SILAC ratios for the quantified proteins. Most quantified proteins presented a SILAC ratio close to 1 as expected for a 1:1 mixture. **(C)** Functional annotation of the 66 altered proteins upon TiO_2-NPs exposure obtained from the gene ontology GO consortium website. Major molecular and biological processes altered included metabolic processes (MP), response to stimulus (RTS), transport (T), gene expression (GE), signalling (S), apoptosis (A), cell cycle regulation (CCR), protein folding (PF), DNA metabolic processes (DMP), response to stress (RTST) and cell proliferation (CP).

consequent upregulation of p53 (Macleod et al., 1995), which induces transcription of cyclin-dependent kinase inhibitor p21 (Gartel and Tyner, 2002), mRNA levels of p53 and p21were also evaluated. While the overexpression of p53 in keratinocytes exposed to TiO_2-NPs was clear, p21 was found inhibited. This result was not expected since p21 plays an essential role in growth arrest after DNA damage (Dulic et al., 1994). In order to validate this result at the protein level, an immunoblot against p21 was carried out and the results also showed a significant inhibition of the protein. This result demonstrated that the inhibition of CDK2, CCNA1 and CCNB1, and thus, the observed cell cycle arrest upon TiO_2-NPs exposure, is not mediated by overexpression of p21. On the other hand, despite the role of p21 as a negative regulator of the cell cycle, it is rarely inactivated in human cancer cells and often displays the expression pattern of an oncogene rather than the one of a tumor suppressor. This paradoxical pattern has been attributed to various activities of p21 other than CDK inhibition (Zhang et al., 1993).

Table 2
Proteins found overexpressed by SILAC upon TiO_2-NPs exposure in HaCaT cells.

Common Name	Accession number	Protein Name	R_{SILAC}	SILAC RSD
SUPT16H	6005757	FACT complex subunit SPT16	5.70	9.62
KRT10	195972866	keratin, type I cytoskeletal 10	3.51	11.33
HNRNPUL2	118601081	heterogeneous nuclear ribonucleoprotein U-like protein 2	3.21	8.89
PPM1G	29826282	protein phosphatase 1G	2.90	3.87
CAV1	15451856	caveolin-1 isoform alpha	2.64	17.77
CLPX	7242140	ATP-dependent Clp protease ATP-binding subunit clpX-like	2.28	18.23
CA2	4557395	carbonic anhydrase 2	2.11	16.60
VPS35	17999541	vacuolar protein sorting-associated protein 35	2.06	18.77
EPRS	62241042	bifunctional glutamate/proline–tRNA ligase	2.05	12.84
PRKCDBP	47132587	protein kinase C delta-binding protein	2.03	19.79
HK1	188497754	hexokinase-1 isoform HKI	1.98	1.03
SAMHD1	38016914	SAM domain and HD domain-containing protein 1	1.97	5.02
VAMP3	4759300	vesicle-associated membrane protein 3	1.95	5.42
PRDX5	6912238	peroxiredoxin-5, mitochondrial isoform a precursor	1.88	19.69
RPLP2	4506671	60S acidic ribosomal protein P2	1.82	3.33
PSME3	388556516	proteasome activator complex subunit 3 isoform 3	1.79	18.56
IPO7	5453998	importin-7	1.69	11.94
FKBP4	4503729	peptidyl-prolyl cis-trans isomerase FKBP4	1.66	13.28
CARS	62240992	cysteine–tRNA ligase, cytoplasmic isoform c	1.65	5.48
RPLP0	4506667	60S acidic ribosomal protein P0	1.64	16.23
PRKCSH	48255889	glucosidase 2 subunit beta isoform 1 precursor	1.63	15.77
FASN	41872631	fatty acid synthase	1.61	11.17
HKDC1	188497750	hexokinase-1 isoform HKI-td	1.59	4.13
RPL29	4506629	60S ribosomal protein L29	1.57	18.28
RUVBL2	5730023	ruvB-like 2	1.56	15.35
SERPINB2	4505595	plasminogen activator inhibitor 2	1.55	18.71
UCHL3	5174741	ubiquitin carboxyl-terminal hydrolase isozyme L3 isoform 2	1.52	6.98
CCT4	38455427	T-complex protein 1 subunit delta isoform a	1.51	14.33
PML1	67089149	protein PML isoform 1	1.51	16.55
PGRMC2	5729875	membrane-associated progesterone receptor component 1	1.51	0.002

Table 3
Proteins found inhibited by SILAC upon TiO_2-NPs exposure in HaCaT cells.

Common Name	Accession number	Protein Name	R_{SILAC}	SILAC RSD
DNAJB11	7706495	dnaJ homolog subfamily B member 11 precursor	−6.44	15.04
SOD2	67782305	superoxide dismutase [Mn], mitochondrial isoform A precursor	−2.71	3.95
EIF4G2	289577080	eukaryotic translation initiation factor 4 gamma 2 isoform 1	−2.51	13.36
SLC9A3R1	4759140	Na(+)/H(+) exchange regulatory cofactor NHE-RF1	−2.19	14.75
TUBB3	50592996	tubulin beta-3 chain isoform 1	−2.14	9.69
RANGAP1	4506411	ran GTPase-activating protein 1	−2.09	8.14
SERPINH1	32454741	serpin H1 precursor	−2.00	18.72
SND1	77404397	staphylococcal nuclease domain-containing protein 1	−1.93	17.14
PLS3	7549809	plastin-3 isoform 1	−1.93	19.02
FAM129A	16757970	protein Niban isoform 2	−1.91	19.89
PACSIN3	19224660	protein kinase C and casein kinase substrate in neurons protein 3	−1.85	1.64
KRT1	119395750	keratin, type II cytoskeletal 1	−1.82	17.79
ACAT1	4557237	acetyl-CoA acetyltransferase, mitochondrial precursor	−1.79	19.94
GLUD1	4885281	glutamate dehydrogenase 1, mitochondrial precursor	−1.78	17.49
EEF1G	4503481	elongation factor 1-gamma	−1.77	10.75
IPO4	62460637	importin-4	−1.73	7.07
MYBBP1A	157694492	myb-binding protein 1A isoform 2	−1.72	14.09
EPS8L2	21264616	epidermal growth factor receptor kinase substrate 8-like protein 2	−1.70	4.13
ATP5L	51479156	ATP synthase subunit g, mitochondrial	−1.69	10.34
NCAPG	21359945	condensin complex subunit 3	−1.68	4.50
LTA4H	4505029	leukotriene A-4 hydrolase isoform 1	−1.68	11.15
HNRNPU	14141161	heterogeneous nuclear ribonucleoprotein U isoform b	−1.67	3.14
CTTN	20357552	src substrate cortactin isoform a	−1.67	18.96
PLEC	41322916	plectin isoform 1	−1.66	17.96
SLC1A5	5032093	neutral amino acid transporter B(0) isoform 1	−1.66	18.63
TOMM34	21361356	mitochondrial import receptor subunit TOM34	−1.65	14.47
KRT7	67782365	keratin, type II cytoskeletal 7	−1.65	19.82
CTSD	4503143	cathepsin D preproprotein	−1.63	19.08
RPL21	18104948	60S ribosomal protein L21	−1.62	9.38
HADHB	4504327	trifunctional enzyme subunit beta, mitochondrial precursor	−1.62	19.15
RPN1	4506675	dolichyl-diphosphooligosaccharide–protein glycosyltransferase	−1.62	16.04
FDPS	4503685	farnesyl pyrophosphate synthase isoform a	−1.61	17.34
ARCN1	11863154	coatomer subunit delta isoform 1	−1.60	14.12
ACTN1	194097350	alpha-actinin-1 isoform a	−1.57	17.69
PTRF	42734430	polymerase I and transcript release factor	−1.54	18.26
EIF4H	11559923	eukaryotic translation initiation factor 4H isoform 1	−1.52	0.29

In fact, it has been described that p21 can act as a negative regulator of the cellular levels of p53 under certain circumstances (Broude et al., 2007), which seems to be the role observed in the present study.

To gain a deeper insight into the toxicity mechanisms associated to TiO_2-NPs exposure in human keratinocytes, a quantitative proteomic approach based on isotopic labeling (SILAC) was used. Out of all the identified proteins, 66 were found deregulated, which are involved in several biological processes including cell cycle regulation, gene expression, metabolic processes or response to stimulus, among others. One of the key steps in understanding the toxicity of a certain type of NPs, is elucidating the cellular internalization mechanism. Previous studies have described different pathways to explain the internalization process, which are mainly caveola-mediated, clathrin-mediated or other receptor-mediated endocytosis (Rauch et al., 2013). Caveola-mediated endocytosis or the “lipid-raft”-dependent process consists of the formation of invaginations in the cell membrane, known as caveolae, where localizes lipids and some important proteins such as dynamin, which enables vesicle scission; cavin, which induces membrane curvature; and caveolin-1 (CAV-1), which is necessary for biogenesis of caveolae (Sahay et al., 2010). Besides, CAV-1 is involved in vesicular transport during caveolae-mediated endocytosis and previous studies have demonstrated that this protein directly binds to Rab-5, which is involved in the transport between the early endosome and the caveosome (Hagiwara et al., 2009). In the present study, CAV-1 (R_{SILAC} = 2.64) appeared highly overexpressed, which might be related with the activation of the caveola-endocytosis pathway upon TiO_2-NPs exposure, and with the TiO_2-NPs aggregates found in exposed HaCaT cells. This is in agreement with a similar study in which CAV-1, together with Cdc42, were demonstrated to be involved in the endocytosis of SiO_2-NPs in HeLa cells (Bohmer and Jordan, 2015). On the other hand, the clathrin-mediated endocytosis is based on the interaction of several proteins with clathrin, which is the main effector of the membrane coating to form vesicles. Other proteins involved in this process are adaptor proteins such as AP2, epsins, dynamins and actin-binding proteins like CTTN (Cao et al., 2003; Samaj et al., 2004; Sauvonnet et al., 2005). CTTN participates in both clathrin-mediated endocytosis, where is needed as a component of clathrin-coated pits, and receptor-mediated endocytosis (Sauvonnet et al., 2005). Interestingly, CTTN (R_{SILAC} = −1.67) was found inhibited in the SILAC experiment, which might preclude the internalization of TiO_2-NPs by the clathrin- or receptor-mediated endocytosis. Additionally, PACSIN3 is a protein involved in vesicles formation and transport. In particular, it is related with the recruitment of proteins that play relevant roles in endocytosis processes. Previous reports have demonstrated that overexpression of PACSIN3 is considered a marker for the activation of the clathrin-mediated endocytosis route, leading to transferrin-mediated endocytosis arrest (Modregger et al., 2000). Based on the previous results, it is not surprising that PACSIN3 was also found inhibited (R_{SILAC} = −1.85). This result, together with the downregulation of a key protein involved in the clathtin-mediated route (CTTN) and the overexpression of CAV-1, support the idea that TiO2-NPs internalize in human keratinocytes by caveola-mediated endocytosis.

Flow cytometry assays have demonstrated that TiO_2-NPs induce cell cycle arrest in exposed human keratinocytes, as it has been already pointed out by previous studies carried out in other types of cells (Saquib et al., 2012; Wang et al., 2015; Wu et al., 2010; Kansara et al., 2015). Thus, it seemed crucial to search for proteins found altered in the SILAC experiment that could shed some light into the specific mechanisms responsible for the TiO_2-NPs-induced cell cycle arrest. Indeed, several deregulated proteins involved in mitosis and cell cycle

progression were found including RanGAP1 ($R_{SILAC} = -2.09$), NCAPG ($R_{SILAC} = -1.68$), EIF4G2 ($R_{SILAC} = -2.51$) and PPM1G ($R_{SILAC} = 2.90$). Ran-binding protein-1 (RanGAP1) stimulate the hydrolysis of GTP to GDP within the Ran GTPase cycle. This cycle includes the control of both, the nucleocytoplasmic transport of important effectors in mitosis regulation, and the RanGTP and RanGDP balance levels. Levels of RanGTP inside the nucleus affect microtubules formation and their appropriate transformation to chromosomes during the interphase (Joseph et al., 2002; Clarke and Zhang, 2008). In addition, RanGAP1 associates with mitotic spindles, which are particularly concentrated at foci near kinetochores; thus, several studies have demonstrated that deregulation of RanGAP1 triggers cell cycle arrest during M phase and deregulation of other proteins involved in cell cycle control (Swaminathan et al., 2004; Chang et al., 2013; Vorpahl et al., 2014). NCAPG is the regulatory subunit of condensin complex, required for conversion of interphase chromatin into mitotic-like condense chromosomes (Kimura et al., 2001). It is well known that this protein is involved in the regulation of the cell cycle and a previous report has shown that knocking down NCAPG provokes cell cycle arrest and impaired cell proliferation. As for EIF4G2, also known as DAP-5, it is involved in the translation of important proteins during mitosis such as Cdk1 or Bcl-2. It has also been demonstrated that EIF4G2 is required for maintaining cell survival during mitosis, and that knocking down EIF4G2 induces M-phase specific caspase-dependent cell death (Marash et al., 2008; Liberman et al., 2009). On the other hand, PPM1G, also known as PP2Cγ, is a serine/threonine phosphatase that regulates the transition phase of cell cycle. Unlike the other above mentioned proteins, PPM1G was found overexpressed in HaCaT cells exposed to TiO_2-NPs. However, several reports have demonstrated that an overexpression of this protein provokes an accumulation of cells in the S phase (Suh et al., 2006), which is in agreement with the flow cytometry results, and with the reduction in mRNA levels found for CDK2 and cyclin A, which are both involved in the S/G2 checkpoint.

TiO_2-NPs are also considered to increase reactive oxygen species (ROS); thus, inducing oxidative stress and an imbalance in the normal redox state of cells (Saquib et al., 2012; Jaeger et al., 2012; Liu et al., 2010). The SILAC experiment has allowed to go further and to identify several proteins that might be responsible for the observed ROS increased and imbalance in TiO_2-NPs exposed cells. Different enzymes with anti-oxidant properties are crucial for controlling the ROS balance. That is the case of SOD2, a mitochondrial protein involved in the conversion of O^{2-} to H_2O_2, which was found inhibited ($R_{SILAC} = -2.71$); thus confirming a potential imbalance of ROS in keratinocytes exposed to TiO_2-NPs. This result is in agreement with the observations carried out by Li et al. in TiO_2-NPs exposed nematodes (Li et al., 2012). Additionally, when cells undergo increased ROS levels and oxidative stress, there are certain proteins that act as a defense mechanism and whose overexpression may be used as an oxidative stress marker. That is the case of the peroxiredoxin protein family. In the SILAC experiment, upregulation of PRDX5 ($R_{SILAC} = 1.88$) was found, which might reduce peroxides with the use of reducing equivalents derived from thioredoxin. It has also been described that TiO_2-NPs cellular uptake cause inflammatory responses (Han et al., 2013; Alinovi et al., 2015). Keratins are important effectors in the control of inflammatory network in keratinocytes; in particular, cytokeratin 1 (KRT1) plays a major role in the epidermal barrier formation and in restricting IL-18 release from keratinocytes. Previous reports showed that a knockdown of KRT1 cause a release of IL-18 and increase of inflammatory factors (Roth et al., 2012). Interestingly, downregulation of KRT1 ($R_{SILAC} = -1.82$) was found upon TiO_2-NPs exposure, which might be one of the causes of the increased inflammatory response observed in TiO_2-NPs exposed cells (Han et al., 2013; Alinovi et al., 2015).

5. Conclusions

In the present work, the toxic effects exerted by TiO_2-NPs in human keratinocytes has been demonstrated. The results have shown how the cellular viability of HaCaT cells is decreased in a concentration-dependent manner, and how TiO_2-NPs induce cell cycle arrest at the S-G2/M phase. These data have been supported by demonstrating inhibition of several key regulators involved in cell cycle progression such as CDK2, CCNA1 and CCNB1. Additionally, downregulation of p21 after TiO_2-NPs exposure has been confirmed, demonstrating that p21 might be acting as a negative regulator of p53 expression in this case. Finally, using quantitative proteomics, several proteins involved in specific pathways and biological processes have been identified, thus helping to understand the mechanisms underlying the observed toxic effects of TiO_2-NPs on human keratinocytes. These findings, have allowed to gain a deeper knowledge of the potential toxicity and the potential risk associated to TiO_2-NPs skin exposure, specially at the molecular level.

Acknowledgements

This work was supported by the Ministerio de Economía y Competitividad grants CTQ2014-55711-R and CTQ2017-85673-R. S. Montalvo-Quiros acknowledges Ministry of Education, Culture and Sports from the Spanish Government for a predoctoral fellowship (FPU13/00723). BSc student J. Garcia is acknowledged for assistance with some of the assays.

Abbreviation list

Arg	Arginine
CDK	Cyclin-dependent kinase
cDNA	complementary Deoxyribonucleic acid
DMEM	Dulbecco's modified Eagle's medium
DMSO	dimethyl sulfoxide
DNA	Deoxyribonucleic acid
EDTA	Ethylenediaminetetraacetic acid
FBS	fetal bovine serum
FITC-Annexin V	Fluorescein isothiocyanate (FITC)-labeled annexin V
GADPH	glyceraldehyde-3-phosphate dehydrogenase
HaCaT	Human adult low Calcium High Temperature Keratinocytes
HEPES	4-(2-hydroxyethyl)-1-piperazineethanesulfonic acid
HPLC	high performance liquid chromatography
HRP	horseradish peroxidase
LC-MS/MS	Liquid chromatography tandem-mass spectrometry
Lys	Lysine
MPs	macrosized particles
mRNA	messenger Ribonucleic acid
MTT	3-(4,5-dimethyl-thiazol-2-yl)2,5-diphenyl tetrazolium bromide
NPs	nanoparticles
PBS	phosphatase saline buffer
PBS-T	phosphatase saline buffer with 0.05% Tween-20
PI	propidium iodide
RNA	Ribonucleic acid
ROS	reactive oxygen species
RT-qPCR	Quantitative Reverse transcription polymerase chain reaction
SDS	sodium dodecyl sulfate
SDS-PAGE	sodium dodecyl sulfate polyacrylamide gel electrophoresis
SILAC	stable isotopic labeling by amino acids in cell culture
TEM	transmission electron microscopy
TiO_2-NPs	Titanium dioxide nanoparticles

Transparency document

Transparency document related to this article can be found online at https://doi.org/10.1016/j.fct.2019.03.036.

References

Alinovi, R., Goldoni, M., Pinelli, S., Campanini, M., Aliatis, I., Bersani, D., Lottici, P.P., Iavicoli, S., Petyx, M., Mozzoni, P., Mutti, A., 2015. Oxidative and pro-inflammatory effects of cobalt and titanium oxide nanoparticles on aortic and venous endothelial cells. Toxicol. Vitro 29, 426–437.

Bohmer, N., Jordan, A., 2015. Caveolin-1 and CDC42 mediated endocytosis of silica-coated iron oxide nanoparticles in HeLa cells. Beilstein J. Nanotechnol. 6, 167.

Broude, E.V., Demidenko, Z.N., Vivo, C., Swift, M.E., Davis, B.M., Blagosklonny, M.V., Roninson, I.B., 2007. CDKN1A) is a negative regulator of p53 stability. Cell Cycle 6, 1468 p21.

Cao, H., Orth, J.D., Chen, J., Weller, S.G., Heuser, J.E., McNiven, M.A., 2003. Cortactin is a component of clathrin-coated pits and participates in receptor-mediated endocytosis. Mol. Cell Biol. 23, 2162.

Chang, K.C., Chang, W.C., Chang, Y., Hung, L.Y., Lai, C.H., Yeh, Y.M., Chou, Y.W., Chen, C.H., 2013. Ran GTPase-activating protein 1 is a therapeutic target in diffuse large B-cell lymphoma. PLoS One 8 e79863.

Chen, Z., Wang, Y., Zhuo, L., Chen, S., Zhao, L., Luan, X., Wang, H., Jia, G., 2015. Effect of titanium dioxide nanoparticles on the cardiovascular system after oral administration. Toxicol. Lett. 239, 123–130.

Clarke, P.R., Zhang, C., 2008. Spatial and temporal coordination of mitosis by Ran GTPase. Nat. Rev. Mol. Cell Biol. 9, 464.

De Matteis, V., 2017. Exposure to inorganic nanoparticles: routes of entry, immune response, biodistribution and in vitro/in vivo toxicity evaluation. Toxics 5, 29.

Dulic, V., Kaufman, W.K., Wilson, S.J., Tlsty, T.D., Lees, E., Harper, J.W., Elledge, S.J., Reed, S.I., 1994. p53-dependent inhibition of cyclin dependent kinase activities in human fibroblasts during radiation-induced G1 arrest. Cell 76, 1013–1023.

Gartel, A.L., Tyner, A.L., 2002. The role of the cyclin-dependent kinase inhibitor p21 in apoptosis. Mol. Cel. Therap. 1, 639.

Gerloff, K., Fenoglio, I., Carella, E., Kolling, J., Albrecht, C., Boots, A.W., Förster, I., Schins, R.P.F., 2012. Distinctive toxicity of TiO_2 rutile/anatase mixed phase nanoparticles on Caco-2 cells. Chem. Res. Toxicol. 25, 646.

Hagiwara, M., Shirai, Y., Nomura, R., Sasaki, M., Kobayashi, K., Tadokoro, T., Yamamoto, Y., 2009. Caveolin-1 activates Rab5 and enhances endocytosis through direct interaction. Biochem. Biophys. Res. Commun. 378, 73.

Han, S.G., Newsome, B., Hennig, B., 2013. Titanium dioxide nanoparticles increase inflammatory responses in vascular endothelial cells. Toxicology 306, 1–8.

Iavicoli, I., Leso, V., Fontana, L., Bergamaschi, A., 2011. Toxicoligical effects of titanium dioxide nanoparticles: a review of in vitro mammalian studies. Eur. Rev. Med. Pharmacol. Sci. 15, 481.

Iavicoli, I., Leso, V., Bergamaschi, A., 2012. Toxicological effects of titanium dioxide nanoparticles: a review of in vivo studies. J. Nanomater. 2012, 1–36.

Jaeger, A., Weiss, D.G., Jonas, L., Kriehuber, R., 2012. Oxidative stress-induced cytotoxic and genotoxic effects of nano-sized titanium dioxide particles in human HaCaT keratinocytes. Toxicology 296, 27.

Jain, A.K., Senapati, V.A., Singh, D., Dubey, K., Maurya, R., Pandey, A.K., 2017. Impact of anatase titanium dioxide nanoparticles on mutagenic and genotoxic response in Chinese hamster lung fibroblast cells (V-79): the role of cellular uptake. Food Chem. Toxicol. 105, 127.

Joseph, J., Tan, S.H., Karpova, T.S., McNally, J.G., Dasso, M., 2002. SUMO-1 targets RanGAP1 to kinetochores and mitotic spindles. J. Cell Biol. 156, 595.

Kansara, K., Patel, P., Shah, D., Shukla, R.K., Singh, S., Kumar, A., Dhawan, A., 2015. TiO_2 nanoparticles induce DNA double strand breaks and cell cycle arrest in human alveolar cells. Environ. Mol. Mutagen. 56, 204.

Khana, M., Naqvib, A.H., Ahmad, M., 2015. Comparative study of the cytotoxic and genotoxic potentials of zinc oxide and titanium dioxide nanoparticles. 2, 765.

Kimura, K., Cuvier, O., Hirano, T., 2001. Chromosome condensation by a human condensin complex in Xenopus egg extracts. J. Biol. Chem. 276, 5417.

Li, Y., Wang, W., Wu, Q., Li, Y., Tang, M., Ye, B., Wang, D., 2012. Molecular control of TiO_2-NPs toxicity formation at predicted environmental relevant concentrations by Mn-SODs proteins. PLoS One 7, 1.

Liberman, N., Marash, L., Kimchi, A., 2009. The translation initiation factor DAP5 is a regulator of cell survival during mitosis. Cell Cycle 8, 204.

Liu, S., Xu, L., Zhang, T., Ren, G., Yang, Z., 2010. Oxidative stress and apoptosis induced by nanosized titanium dioxide in PC12 cells. Toxicology 267, 172.

Luque-Garcia, J.L., Sanchez-Diaz, R., Lopez-Heras, I., Martin, P., Camara, C., 2013. Bioanalytical strategies for in-vitro and in-vivo evaluation of the toxicity induced by metallic nanoparticles. Trends Anal. Chem. 43, 254.

Macleod, K.F., Sherry, N., Hannon, G., Beach, D., Tokino, T., Kinzler, K., Vogelstein, B., Jacks, T., 1995. p53-dependent and independent expression of p21 during cell growth, differentiation and DNA damage. Genes Dev. 9, 935.

Marash, L., Liberman, N., Henis-Korenblit, S., Sivan, G., Reem, E., Elroy-Stein, O., Kimchi, A., 2008. DAP5 promotes cap-independent translation of Bcl-2 and CDK1 to facilitate cell survival during mitosis. Mol. Cell. 30, 447.

Márquez-Ramírez, S.G., Delgado-Buenrostro, N.L., Chirino, Y.I., Iglesias, G.G., López-Marure, R., 2012. Titanium dioxide nanoparticles inhibit proliferation and induce morphological changes and apoptosis in glial cells. Toxicology 302, 146–156.

Modregger, J., Ritter, B., Witter, B., Paulsson, M., Plomann, M., 2000. All three PACSIN isoforms bind to endocytic proteins and inhibit endocytosis. J. Cell Sci. 4521, 4511.

Rauch, J., Kolch, W., Laurent, S., Mahmoudi, M., 2013. Big signals from small particles: regulation of cell signaling pathways by nanoparticles. Chem. Rev. 113, 3391.

Ren, Y., Liu, X., Geng, R., Lu, Q., Rao, R., Tan, X., Yang, X., Liu, W., 2018. Increased level of α2,6-sialylated glycans on HaCaT cells induced by titanium dioxide nanoparticles under UV radiation. Nanomaterials 8, E253.

Roth, W., Kumar, V., Beer, H.D., Richter, M., Wohlenberg, C., Reuter, U., Thiering, S., Staratschek-Jox, A., Hofmann, A., Kreusch, F., Schultze, J.L., Vogl, T., Roth, J., Reichelt, J., Hausser, I., Magin, T.M., 2012. Keratin 1 maintains skin integrity and participates in an inflammatory network in skin through interleukin-18. J. Cell Sci. 125, 5269.

Sahay, G., Alakhova, D.Y., Kabanov, A.V., 2010. Endocytosis of nanomedicines. J. Control. Release 145, 182.

Samaj, J., Baluska, F., Voigt, B., Schlicht, M., Volkmann, D., Menzel, D., 2004. Endocytosis, actin cytoskeleton, and signaling. Plant Physiol. 135, 1150.

Saquib, Q., Al-Khedhairy, A., Siddiqui, M., Abou-Tarboush, F.M., Azam, A., Musarrat, J., 2012. Titanium dioxide nanoparticles induced cytotoxicity, oxidative stress and DNA damage in human amnion epithelial (WISH) cells. Toxicol. Vitro 26, 351.

Sauvonnet, N., Dujeancourt, A., Dautry-Varsat, A., 2005. Cortactin and dynamin are required for the clathrin-independent endocytosis of γc cytokine receptor. J. Cell Biol. 168, 155.

Shi, H., Magaye, R., Castranova, V., Zhao, J., 2013. Titanium dioxide nanoparticles: a review of current toxicological data. Part. Fibre Toxicol. 10, 15.

Suh, E.J., Kim, T.Y., Kim, S.H., 2006. PP2C-mediated S-phase accumulation induced by the proteasome-dependent degradation of p21WAF1/CIP1. FEBS Lett. 580, 6100.

Swaminathan, S., Kiendl, F., Körner, R., Lupetti, R., Hengst, L., Melchior, F., 2004. RanGAP1*SUMO1 is phosphorylated at the onset of mitosis and remains associated with RanBP2 upon NPC disassembly. J. Cell Biol. 164, 965.

Tucci, P., Porta, G., Agostini, M., Dinsdale, D., Iavicoli, I., Cain, K., Finazzi-Agró, A., Melino, G., Willis, A., 2013. Metabolic effects of TiO_2 nanoparticles, a common component of sunscreens and cosmetics, on human keratinocytes. Cell Death Dis. 4, 549.

Uboldi, C., Urban, P., Gilliland, D., Bajak, E., Valsami-Jones, E., Ponti, J., Rossi, F., 2016. Role of the crystalline form of titanium dioxide nanoparticles: rutile, and not anatase, induces toxic effects in Balb/3T3 mouse fibroblasts. Toxicol. Vitro 31, 137.

Valentini, X., Absil, L., Laurent, G., Robbe, A., Laurent, S., Muller, R.N., Legrand, A., Nonclercq, D., 2017. Toxicity of TiO2 nanoparticles on the NRK52E renal cell line. Mol. Cell Toxicol. 13, 419–431.

Valentini, X., Deneufbourg, P., Paci, P., Rugira, P., Laurent, S., Frau, A., Stanicki, D., Ris, L., Nonclercqa, D., 2018. Morphological alterations induced by the exposure to TiO_2 nanoparticles in primary cortical neuron cultures and in the brain of rats. Toxicol Rep 5, 878.

Vorpahl, M., Schönhofer-Merl, S., Michaelis, C., Flotho, A., Melchior, F., Wessely, R., 2014. The Ran GTPase-activating protein (RanGAP1) is critically involved in smooth muscle cell differentiation, proliferation and migration following vascular injury: implications for neointima formation and restenosis. PLoS One 9 e101519.

Wang, Y., Cui, H., Zhou, J., Li, F., Wang, J., Chen, M., Liu, Q., 2015. Cytotoxicity, DNA damage, and apoptosis induced by titanium dioxide nanoparticles in human non-small cell lung cancer A549 cells. Environ. Sci. Pollut. Res. 22, 5519.

Wright, C., Iyer, A.K., Wang, L., Wu, N., Yakisich, J.S., Rojanasakul, Y., Azad, N., 2017. Effects of titanium dioxide nanoparticles on human keratinocytes. Drug Chem. Toxicol. 40, 90.

Wu, J., Sun, J., Xue, Y., 2010. Involvement of JNK and P53 activation in G2/M cell cycle arrest and apoptosis induced by titanium dioxide nanoparticles in neuron cells. Toxicol. Lett. 199, 269.

Zhang, H., Xiong, Y., Beach, D., 1993. Proliferating cell nuclear antigen and p21 are components of multiple cell cycle kinase complexes. Mol. Biol. Cell 4, 897.